

## Fabrication and photocatalytic properties of ceramic ZnS nanocomposites

Soon-Do Yoon<sup>a,†</sup>, Jeong Woo Yun<sup>b,†</sup> and Yeon-Hum Yun<sup>c,d,\*</sup>

<sup>a</sup>Department of Chemical and Biomolecular Engineering, Chonnam National University, Yeosu, Jeonnam 59626, South Korea

<sup>b</sup>School of Chemical Engineering, Chonnam National University, Gwangju 61186, South Korea

<sup>c</sup>Department of Energy & Resources Engineering, Chonnam National University, Gwangju 61186, South Korea

<sup>d</sup>Geoconvergence Research Center, Chonnam National University, Gwangju 61186, South Korea

Ceramic ZnS nanocomposites were prepared by mechanical processing and one-step heat sintering with powder mixtures of fly ash, waste glass, and ZnS (template-free hydrothermal method manufacturing). Chemical durability and morphological characteristics of heat-treated samples at 800 °C with/without acid treatment were evaluated. The photocatalytic activities were estimated with methyl orange (MO), methylene blue (MB), acetaldehyde (ATA), and 2,4-dichlorophenoxyacetic acid (2,4-D) as photodegradation targets. Crystallization behaviors of the prepared ceramic ZnS nanocomposites were investigated using X-ray diffraction (XRD), field emission-scanning electron microscopy (FE-SEM), and energy dispersive X-ray spectrometry (EDS). In addition, compressive and bending strength as mechanical properties were evaluated. Ceramic ZnS nanocomposites were found to show improvement in optimal photocatalytic reaction and physical properties regardless of acid treatment when the amount of ZnS nanoparticles was increased from 7.0 to 25.0 wt%. Degrees of photocatalytic decomposition of MO, ATA, 2,4-D, and MB by acid treated ceramic ZnS nanocomposites containing 25 wt% ZnS were about 0.185, 0.121, 0.216, 0.236, respectively, after UV irradiation for 180 min.

**Keywords:** Ceramic ZnS nanocomposite, Chemical durability, Acid treatment, Photocatalytic activity, Mechanical properties

### Introduction

ZnS (zinc sulfide), one of metal sulfides, has attracted a lot of attention in various fields because it can be used to produce high-efficiency photocatalysts with thermodynamically optimal conditions for photocatalytic redox reactions and appropriate band potential of electricity [1-3]. It is a very important transition metal sulfide that can be used as many practical applications such as electroluminescent phosphors [4-5], electro-photocatalysts [6-7], and optoelectronic devices [8-9].

Photocatalytic processes in nanoscale materials mostly require diffusion or coating of a suitable substrate for functional performance. However, nanoscale photocatalysts used in dispersion methods are difficult to assemble after use. To solve this problem, photocatalysts in which ZnS layers are formed by coating various substrates (such as ceramics, glass plates, metal plates, or glass tubes) or by sol-gel processes have recently been developed [10-12]. Additionally, nanocomposites added ZnS nanoparticles can be prepared to have various physicochemical, thermal, and other distinctive properties with superior advantages. Nanocomposites have properties superior to conventional micro-scale composite materials.

It can be also synthesized using simple and inexpensive methods [13-14]. In many studies, nanocomposites that represent composite materials with nanometer particle sizes have been fabricated using nanoclay, nanofiller, nanofibril, or nanoSiO<sub>2</sub>. Song et al. [15] and Lai et al. [16] have reported that mechanical, chemical, thermal properties, and water-proof functions of prepared nanocomposites were improved by the addition of nanoparticles.

The main objective of this study was to prepare ceramic ZnS nanocomposites using waste glass powders, fly ash from thermal power plants, ZnS nanoparticles as inorganic fillers in matrix of the composite materials and to evaluate their mechanical, chemical durability and photocatalytic properties. Properties of nano-ZnS of ceramic composites are known to depend essentially on properties of finely precipitated ZnS crystals and the residual phase. Therefore, it is expected that these ceramic ZnS nanocomposites would exhibit excellent photocatalytic activities if nano-ZnS crystals could be densely deposited in ceramic complexes containing ZnS crystals. Advanced microscale composite materials with appropriately well-developed properties can have various ripple effects if they are prepared by economically reasonable methods. In this respect, it is significant point that recycling of waste resources such as fly ash and waste glass can improve various environmental problems. For this reason, they can be obtained by modifying inefficient chemical bonding

\*Corresponding author:  
Tel : +82-61-659-7297  
Fax: +82-61-659-7299  
E-mail: yhhumm@empas.com

†These authors contributed equally to this work.

with a high temperature heat sintering step, using a disc-type ball mill, a unique mechanical bonding process [17]. In order to verify the applicability which can respond to environmental changes as an acidic condition, we also evaluated the chemical durability of ceramic ZnS nanocomposites prepared by acidic treatment. The characterization such as crystallinity and morphology of ceramic ZnS nanocomposites prepared with different ZnS nanoparticles content were analyzed using X-ray diffractometer (XRD) and field emission scanning electron microscopy (FE-SEM). Energy dispersive X-ray spectroscopy (EDS) was also used to observe and analyze their chemical compositions of ceramic ZnS nanocomposites. Physical properties such as compressive strength, bending strength and Vickers hardness of these fabricated ceramic ZnS nanocomposites were investigated. Additionally, photocatalytic degradation of methyl orange (MO), acetaldehyde (ATA), 2,4-dichlorophenoxyacetic acid (2,4-D), and methylene blue (MB) as photodegradation targets was measured using the ceramics ZnS nanocomposites under UV light irradiation.

## Experimental

ZnS nanoparticles were synthesized by the template-free hydrothermal method [18]. In a typical method for synthesizing ZnS, 10.0 mmol  $\text{Zn}(\text{CH}_3\text{COO})_2$  (Aldrich Chemical Company, Inc., USA) and 10 mmol  $\text{Na}_2\text{S}_2\text{O}_3 \cdot 5\text{H}_2\text{O}$  (Aldrich Chemical Company, Inc., USA) were dissolved in 110 mL of deionized water (DW) under continuous stirring for 50 min. The pH was then controlled, and the mixture was transferred to a teflon-lined autoclave with 125 mL capacity. The autoclave was maintained at 150 °C for 10 h and then cooled to room temperature. The precipitate was washed several times with distilled water (DW) and absolute ethanol to remove soluble inorganic impurities. Fly ash from municipal waste incinerator (Yeocheon, South Korea) and waste glass cullet mixed with several types of waste glass (bottles, car window shields, plates, etc.) were used as raw materials.

Chemical compositions of raw materials, fly ash and waste glass cullet are listed in Table 1. According to chemical analysis, fly ash was composed of oxide (wt%); 46.31%  $\text{SiO}_2$ , 27.58%  $\text{CaO}$ , 8.81%  $\text{MgO}$ , 13.56%  $\text{Al}_2\text{O}_3$ , and 6.44%  $\text{Fe}_2\text{O}_3$ . Energy dispersive X-ray spectrometer (EDS, X-Max, Oxford Ins., UK) was used for elemental analysis. In these experiments, a fine fly ash powder (about 200 mesh) from a municipal waste incinerator was used. Glass cullet was carefully washed

in a water bath to remove contaminants and dried in a dry oven at 90 °C for 24 h. Glass powder was obtained by grinding the glass cullet in a disk type ball mill (Retsch GmbH & Co.KG, D-42781 HAAN, TYPE: RS1, Germany) for 20 minute (700 rpm). Ceramic ZnS nanocomposites were attained by mechanical processing using the milling technique. Firstly, the powder mixture consisted of waste glass powder (65 wt%) and fly ash (35 wt%). Approximately 30 g of two different powder mixtures of waste glass and fly ash were mechanically ground in a disk-type ball mill for 8 hours (700 rpm). After grinding, the particle size was decided with a particle size analyzer (PSA, Malvern Ins. Lab., MS 1002). Most particles were in the range of 0.1-1  $\mu\text{m}$ . ZnS nanoparticles (0, 7, 14, 20, and 25 wt%) were then mixed directly together using a mixer for 20 min. These mixtures were pressed into a cylindrical shape with a diameter of 10 mm and a length of 30-50 mm without using a binder. Formed samples were fired to 800 °C at a heating rate of 5 °C /min for 1 h under air and in a box-type SiC furnace. They were then allowed to cool inside the furnace. The chemical durability for acidic conditions was evaluated by the measurement of weight change. To investigate the chemical durability, the ceramic ZnS nanocomposite specimens were immersed into 30 mL acidic solution (1 N  $\text{H}_2\text{SO}_4$ ) at 50 °C for 48 h. After immersing, the specimens were washed with DW and dried at 80 °C for 20 h.

Surface morphology and compositions of these ceramic ZnS nanocomposites were evaluated using field emission scanning electron microscopy (FE-SEM, ZEISS Sigma 500, Carl Zeiss Co., Ltd, Germany) equipped with an energy dispersive X-ray spectrometer (EDS) that has a Robinson type backscattered electron detector. An X-ray diffraction analysis for ceramics ZnS nanocomposites was performed using  $\text{Cu K}_\alpha$  radiation by scanning at a rate of 2 degrees/min with a diffractometer (XRD, Rigaku D/MAX Ultima III). The scan speed was 2°/min, and the scan range of the diffraction angle ( $2\theta$ ) was  $15^\circ \leq 2\theta \leq 60^\circ$ . Photoluminescence (PL) spectroscopy ( $f = 0.5$  m, Acton Research Co., Spectrograph 500i, USA) was performed at room temperature a 266 nm DPSS laser (Photoluminescence Measurement System, Gwangju center, KBSI), and an intensified CCD (PI-MAX3) (Princeton Instrument Co., IRY1024, USA) at a room temperature.

Density was examined using an Electronic Densimeter (ED-120T, MFD BY A&D CO., LTD, Japan). Compressive strength was determined with a universal tester (Instron 4302, Instron Co., England). Bending strength was investigated with a 3-point bending strength

**Table 1.** Density and weight change% of ceramics nanocomposites in regard to ZnS contents (0, 7, 14, 20, and 25 wt%)

	Without ZnS	7 wt%	14 wt%	20 wt%	25 wt%
Density ( $\text{g}/\text{cm}^3$ )	2.573	2.385	2.631	2.369	2.296
Weight change% (1N $\text{H}_2\text{SO}_4$ )	0.132	0.148	0.151	0.137	0.141

**Table 2.** The kinetic constants ( $k_1$ ) and correlation coefficients ( $R^2$ ) of the pseudo-first-order model for the liner plots of ceramic nanocomposites added ZnS nanoparticles (before and after acid immersion)

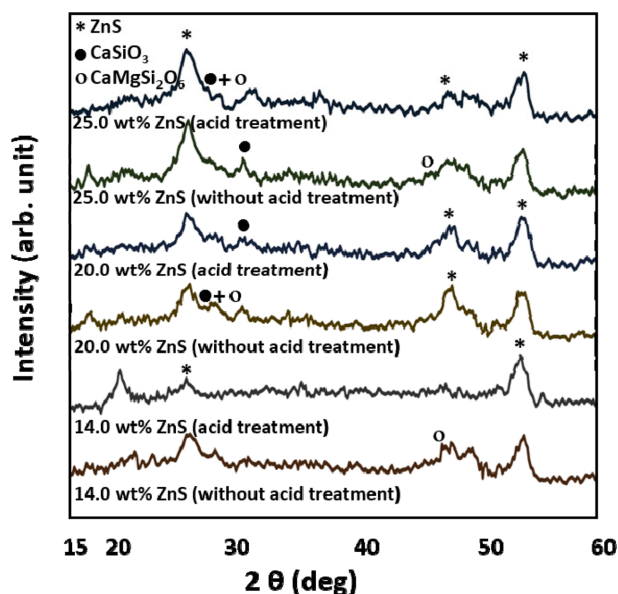
Photodegradation targets (ZnS wt%)		Kinetic constants ( $k_1$ )	Correlation coefficients ( $R^2$ )
MO	Before acid immersion	0.154 min <sup>-1</sup>	0.996
(ZnS 25 wt%)	After acid immersion	0.139 min <sup>-1</sup>	0.994
ATA	Before acid immersion	0.145 min <sup>-1</sup>	0.990
(ZnS 25 wt%)	After acid immersion	0.162 min <sup>-1</sup>	0.995
2,4-D	Before acid immersion	0.131 min <sup>-1</sup>	0.986
(ZnS 25 wt%)	After acid immersion	0.148 min <sup>-1</sup>	0.988
MB	Before acid immersion	0.126 min <sup>-1</sup>	0.991
(ZnS 25 wt%)	After acid immersion	0.134 min <sup>-1</sup>	0.989

test using a universal tester (Instron N8872, Instron Co., England). Vickers hardness was estimated using a Vickers hardness tester (Shimadzu Co., HMV-2 series, Japan). To examine chemical durability, ceramic nanocomposites were immersed into 15 mL acidic solution (1 N H<sub>2</sub>SO<sub>4</sub>) at 60 °C for 48 h. After immersing, specimens were washed with distilled water and dried at 80 °C for 12 h.

Photocatalytic degradation for methyl orange (MO, Aldrich Chemical Company, Inc., USA) and 2,4-dichlorophenoxyacetic acid (2,4-D, Aldrich Chemical Company, Inc., USA), acetaldehyde (ATA, Carlo Erba (Milan, Italy)), and methylene blue (MB, Junsei Chemical, Japan) were performed using the method described by Yun et al. [19]. Briefly, photocatalytic degradability of BPA, 2,4-D, MB, and MO for the prepared ceramic ZnS nanocomposite were examined using a decomposition test in an aqueous solution under UV light. Photocatalytic decomposition of target compounds was calculated as the ratio of initial ( $C_0$ ) and final concentration ( $C$ ). The initial concentration of BPA, 2,4-D, MB, and MO was 10 ppm. UV illumination was carried out with two UV-A lamps (F10T8BLB, Sankyo Denki). Concentrations of BPA, 2,4-D, MB, and MO were investigated by absorbance measurement with a UV-vis. spectrophotometer (Optizen 2120UV, Neogen Co., Ltd, Korea). In case of ATA, it was evaluated using a GC/MS (Gas Chromatography Mass Spectrometer, QP-5050A, Shimadzu). Each sample and 1 mL ATA were placed into a reactor. Dark condition was then maintained until ATA was adsorbed to the sample surface for 3 h. When ATA changes no longer appeared on the specific peak of ATA on GC/MS, UV lamp was radiated.

## Results and Discussion

Fig. 1 represents the results of XRD patterns of ceramic nanocomposites containing ZnS nanoparticles (14% and 25 wt%) before and after immersing in acidic solution. Crystalline phases present in ceramic ZnS nanocomposites corresponded to ZnS (JCPDS File 05-0566), CaSiO<sub>3</sub> (JCPDS File 76-0925), and CaMgSi<sub>2</sub>O<sub>6</sub> (JCPDS File 78-1390). ZnS diffraction patterns showed

**Fig. 1.** X-ray diffraction patterns of ceramic ZnS nanocomposites with/without acid treatment.

$2\theta$  value main peaks of 28.67°, 47.61°, and 56.42° corresponding to ZnS. The intensity of ZnS distinctive peak was increased as the amount of ZnS added to the ceramic nanocomposite increased. This designates that ZnS is included in the specimen. The variation in ZnS phase did not detect after blending ZnS nanoparticles into ceramic nanocomposites (non-acid & acid treatment). The results indicate that the prepared ceramic ZnS nanocomposite has photocatalytic activity because the characteristic peaks of ZnS with a relatively high photocatalytic activity were observed even when it is combined with the ceramic nanocomposite. Peak intensities corresponding to the CaSiO<sub>3</sub> + CaMgSi<sub>2</sub>O<sub>6</sub>, CaSiO<sub>3</sub>, and CaMgSi<sub>2</sub>O<sub>6</sub> crystal were still identified in specimens. It is significant to note that these peak intensities are due to the formation of wollastonite and diopside crystals. The formation of the crystal phase at annealing temperature of 800 °C has a sufficient effect on physically mechanical properties. From the results, it can be verified that the crosslinking is occurred by heat sintering between nanocomposites components. To gain more insight into chemical durability, morpho-

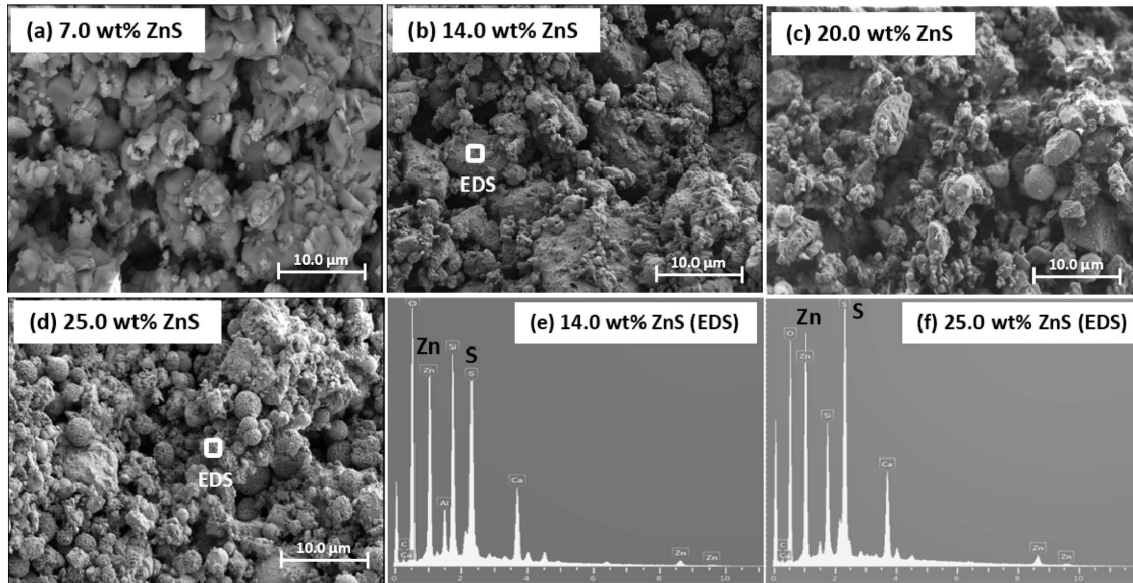


**Fig. 2.** FE-SEM images EDS analyses of ceramic nanocomposites added ZnS nanoparticles (Before acid immersion): (a) 7 wt%, (b) 14 wt%, (c) 20 wt%, (d) 25 wt%, (e) 14 wt% EDS, and (f) 25 wt% EDS.

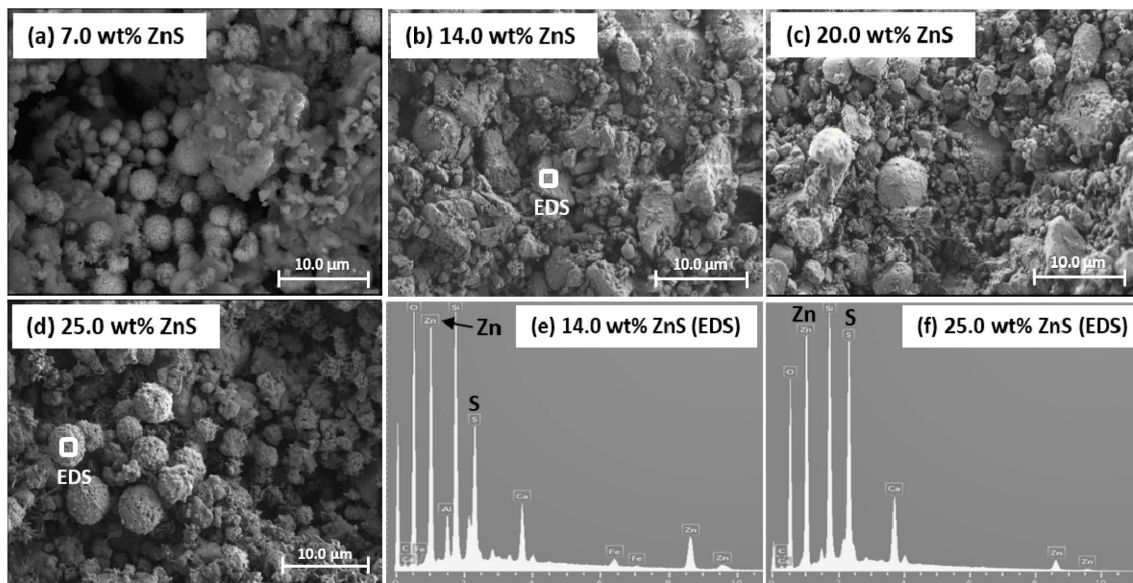


**Fig. 3.** FE-SEM images EDS analyses of ceramic nanocomposites added ZnS nanoparticles (After acid immersion): (a) 7 wt%, (b) 14 wt%, (c) 20 wt%, (d) 25 wt%, (e) 14 wt% EDS, and (f) 25 wt% EDS.

logical and chemical compositions of the grain-like phase at surfaces of specimens before and after immersing in acidic solution were examined by FE-SEM and EDS. Figs. 2 and 3 show surface morphologies and grain-like phase's chemical compositions of ceramic nanocomposites containing ZnS nanoparticles (7.0–25.0 wt%) before and after acid-immersion. Figs. 2a, b, c, and d present the results of morphological analysis of the specimens added with ZnS nanoparticles before acid-immersion. Fig. 2a shows many rough angular-shape grains at size of 2.6  $\mu\text{m}$  to 8.9  $\mu\text{m}$  with irregular type grains in the matrix. The grain's surface shape was heterogeneous and small in size. As seen in

Figs. 2b and 2c, when ceramic nanocomposites were added with ZnS nanoparticles at 14.0 and 20.0 wt%, surfaces of specimens revealed irregular and unsystematic round-like grains with size ranging from 2.3  $\mu\text{m}$  to 7.6  $\mu\text{m}$ . A morphological analysis of specimens with ZnS contents of 25.0 wt% (Fig. 2d) showed that round-shape grains unchangeably aggregated in the matrix before immersing in acidic solution. It was caused by the formation of highly crystallized ZnS nanoparticles, and the round-shape crystals are typical SEM results of ZnS.

The chemical durability of nanocomposites investigated by observing surfaces of samples with various ZnS

contents (7.0-25.0 wt%) after immersing in acidic solution is shown in Fig. 3. Chemical durability was not significantly affected by the acid treatment and ZnS contents (Fig. 3a, b, c, and d), and no noticeable change was seen when compared to Fig. 2. When FE-SEM images were obtained for ceramic nanocomposites prepared by adding ZnS nanoparticles with heat sintering at 800 °C, no difference in chemical durability was found between before and after acid treatment of the samples. As clearly shown in Figs. 2 and 3, gradual increase in ZnS content caused a change in grain shape and surface condition of the specimen regardless of acid treatment. Therefore, an important factor for the crystal formation and surface state of the nanocomposite is the change in ZnS content. From the results of EDS analysis, Si, Zn, S, Ca, Al and Fe were detected on grain-like phase's surfaces of all specimens before and after acid-immersion. As shown in Figs. 2f and e, relatively major and strong peak intensities corresponding to zinc and sulfur were identified on surface grains for non-acid treated specimens. Results of EDS of ceramic nanocomposites after acid treatment are shown in Figs. 3e and f. It is very difficult to identify variations in zinc and sulfur peak intensities between before (Figs. 2e and f) and after (Figs. 3e and f) acid-immersion. In case of specimens added ZnS nanoparticles, nanoparticles were closely agglomerated on specimens and crystallized, so that no significant change in grain-like crystals' EDS peak intensities between non-acid and acid treatment was detected.

Compressive and bending strength were investigated for specimens added 0, 7.0, 14.0, 20.0 and 25.0 wt% ZnS nanoparticles in ceramic ZnS nanocomposites sintered by heating at 800 °C. For all specimens, compressive and bending strength before immersion (BI) and after immersion (AI) in the acidic solution are shown according to the degree of increase of ZnS content in the nanocomposite. Tests were executed 20 times for each specimen and the results are shown in Fig. 4. As seen in Figs. 4a and b, compressive strengths of ceramic ZnS nanocomposites before and after acid treatment with the increase of ZnS content ranged from 117.3 to 154.9 MPa (BI) and from 103.9 to 150.8 MPa (AI), respectively. In addition, bending strength was improved from 36.5 to 73.9 MPa (BI) and from 29.4 to 65.8 MPa (AI). These specimens after acid treatment tended to have slightly lower all strengths, although they showed sufficiently good outcomes. Figs. 4a and b show that the increase in compressive and bending strengths of ceramic nanocomposites (25.0 wt% ZnS) is due to an increase in content of ZnS nanoparticles contained in the sample regardless of acid treatment. These results confirmed that ZnS nanoparticles contained in ceramic nanocomposites could play a crosslinking of the components, thus ceramic ZnS nanocomposites showed outstanding mechanical strengths when ZnS content was increased. Fig. 4c shows Vickers hardness

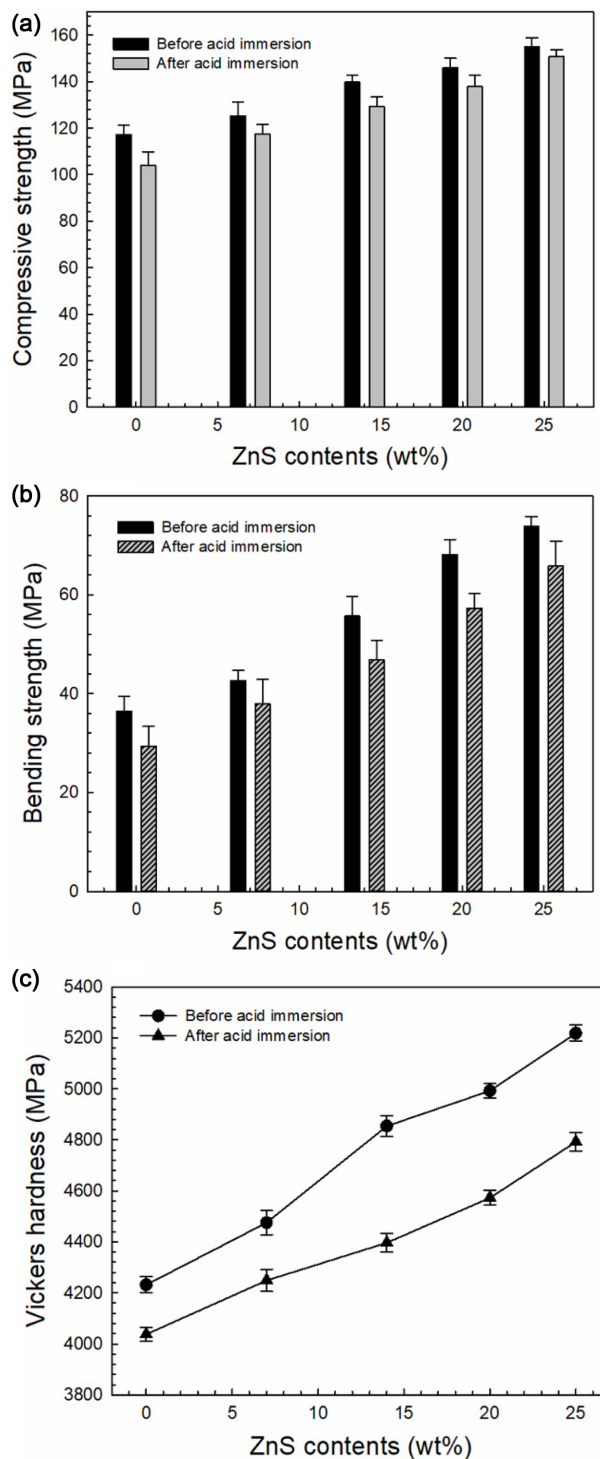


**Fig. 4.** Physical properties of ceramics nanocomposites with added ZnS nanoparticles contents (0, 7, 14, 20, and 25 wt% ZnS contents); before acid immersion and after acid immersion. (a) Compressive strength (MPa) of the prepared ceramics nanocomposites. (b) Bending strength (MPa) of the prepared ceramics nanocomposites. (c) Vickers hardness (MPa) of the prepared ceramics nanocomposites.

for heat-treated ceramic ZnS nanocomposites with different ZnS content (before and after acid treatment). It was certain that the value of Vickers hardness

increased as the content of ZnS nanoparticles increased from 0 to 25.0 wt%. As shown in Fig. 4c, ceramic nanocomposites heat-treated at 800 °C (25.0 wt% ZnS) had the maximum hardness values of  $5218.4 \pm 32$  MPa before acid treatment and  $4792.5 \pm 36$  MPa after acid treatment. These results indicate that the development and technological improvement of ZnS nanoparticles (increasing the content of ZnS) could make them well dispersed in ceramic nanocomposites to improve both compressive and bending strengths so that specimens with different contents of ZnS nanoparticles could have sufficient mechanical strength and were suitable for practical usage.

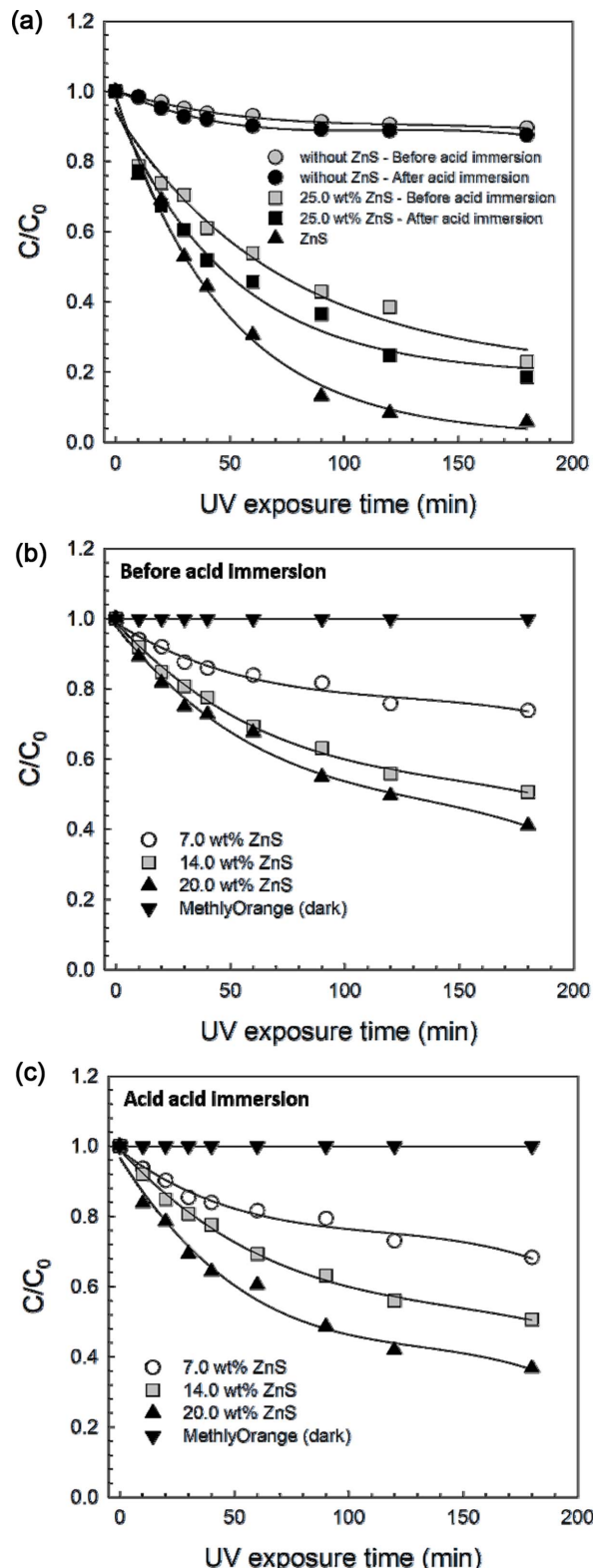
Table 1 show density and weight changes (%) before and after acid treatment of specimens (ZnS content: 0, 7.0, 14.0, 20.0, and 25.0 wt%) heat-treated at 800 °C. To calculate weight changes, the degree of weight changes (%) was defined as follows:

$$\text{Weight changes (\%)} = (m_1 - m_2) / m_1 \times 100$$

where  $m_1$  and  $m_2$  were weights of specimens before and after immersing in the acidic solution [20], respectively. Changes in the density and weight of specimens with increasing ZnS content were not affected by acid treatment. The change in weight before and after acid immersion was very small, making it difficult to determine the exact chemical durability of the specimens. Thus, the change in chemical durability of the specimen due to weight gain could not be evidently explained.

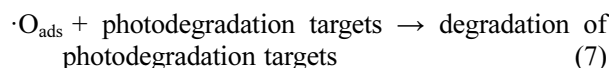
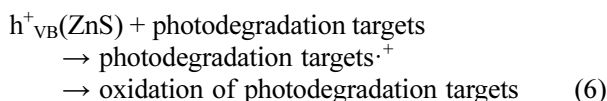
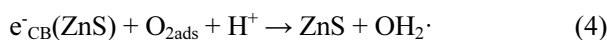
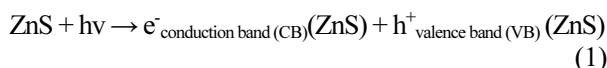
Photocatalytic activities of acid treated and non-acid treated ceramic nanocomposites with/without the addition of ZnS nanoparticle were examined based on the decomposition degree ( $C/C_0$ ) of MO as a photodegradation target under UV light. Prepared specimens were irradiated with UV light having a broad emission spectrum of 315-400 nm. The maximum illumination was yielded at 352 nm.

Fig. 5 shows the photocatalytic degradability of MO in acid treated and non-acid treated ceramic nanocomposites with/without adding ZnS nanoparticle as a function of UV irradiation time. The variation in MO photocatalytic degradation was visibly observed with ZnS nanoparticles and ceramic nanocomposites added ZnS nanoparticle contents although the photocatalytic degradability of MO on ZnS nanoparticle was superior to ceramic nanocomposites containing ZnS (Fig. 5a). The degradation by UV irradiation also confirmed that MO decomposition increased with increasing ZnS content in all cases acid treated ceramic ZnS nanocomposites (Fig. 5b) and non-acid treated ceramic ZnS nanocomposites (Fig. 5c). From the results, we found that the photocatalytic decomposition ( $C/C_0$ ) of MO in ceramics nanocomposites added with 20.0 and 25.0 wt% ZnS were about 0.410 and 0.229 before acid treatment, 0.367 and 0.185 after acid treatment, respectively. For acid treated ceramic ZnS nanocomposites, the reason why photocatalytic decomposition of the



**Fig. 5.** Photocatalytic degradation and kinetic linear simulation of methyl orange (MO) under UV irradiation. (a) Photocatalytic degradation and kinetic linear simulation of MO for ceramic nanocomposites with/without the addition of ZnS nanoparticles and acid treatment. (b) Photocatalytic degradation and kinetic linear simulation of MO for ceramic ZnS nanocomposites prepared with ZnS content before acid immersion. (c) Photocatalytic degradation and kinetic linear simulation of MO for ceramic ZnS nanocomposites prepared with ZnS content after acid immersion.

MO was slightly superior was found to be due to difference in the decomposition of the MO because pores and specific surface areas were generated after acid treatment of ceramic nanocomposites. The photocatalytic mechanism can be explained as follows. The positive holes and electrons generated by UV light on the ZnS are attributed to the hydroxyl radicals formation. The photocatalytic reaction between the electrons and the  $H_2O_{ads}$  forms  $\cdot OH_{ads}$ ,  $OH_{ads}^-$ , and  $HO_2\cdot$  as the hydroxyl species. The OH formed by electrons is shown by the following Eq. (1)-(7). Then, photodegradation targets are degraded by the attack of direct hole and hydroxyl species [21, 22].



The photocatalytic decomposition of ATA, 2,4-D and MB in acid treated and non-acid treated ceramic nanocomposites added 25.0 wt% ZnS as a function of UV irradiation time is shown in Fig. 6. It was confirmed that the  $C/C_0$  significantly decreased with UV irradiation time. When compared to non-acid and acid treated specimens, the effect of photocatalytic activity of acid treated specimens was found to be higher than that without acid treatment. To further compare the decomposition efficiency of photodegradation targets, we investigated the pseudo-first order kinetic model. The kinetic constant was calculated using a pseudo-first-order equation [Eq. (8)] and a simplified version of the Lagergren equation [Eq. (9)]. Lagergren [23] has proposed a rate equation for the sorption of a solute. It was established based on the adsorption capacity. The Lagergren equation is the most generally used rate equation in sorption. This kinetic model is expressed as follows:

$$\frac{dq_t}{dt} = k_1(q_e - q_t) \quad (8)$$

Integrating the above equation for the boundary conditions  $t = 0$  to  $t = t$  and  $q_t = q_t$  gives:

$$\ln(q_e - q_t) = \ln(q_e - k_1 t) \quad (9)$$

The kinetic constant  $k_1$  ( $\text{min}^{-1}$ ) was determined by plotting  $\ln(q_e - q_t)$  versus  $t$  or  $\ln(q_e - q_t)/q_e$  versus  $t$ . From these results, the correlation coefficients ( $R^2$ ) of

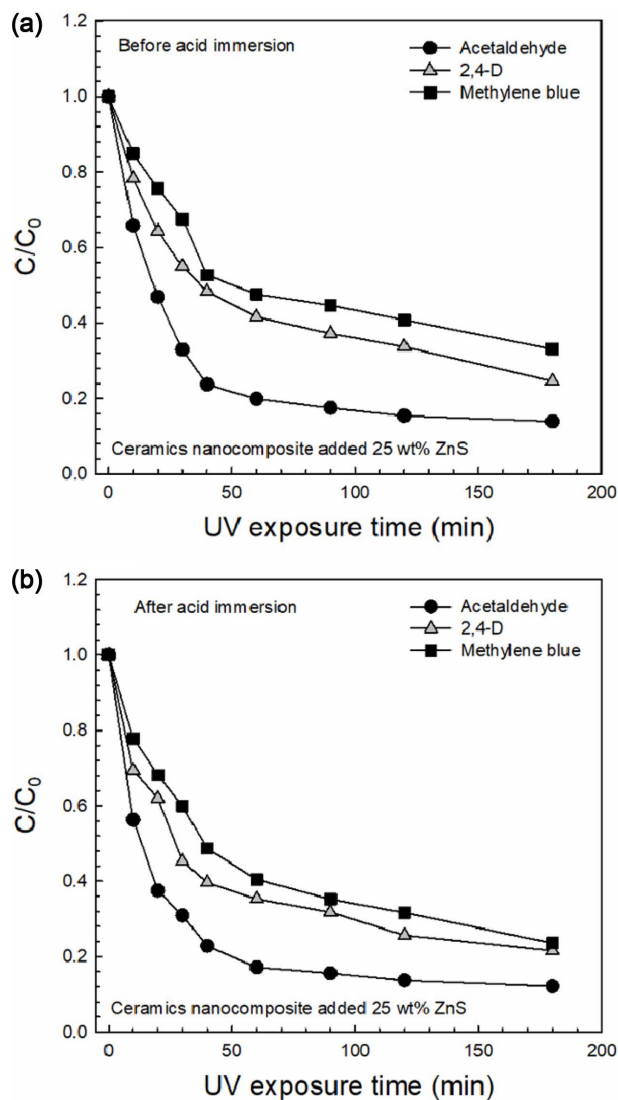


**Fig. 6.** Photocatalytic degradation of acetaldehyde (ATA), 2,4-dichlorophenoxyacetic acid (2,4-D), methylene blue (MB) in the ceramic nanocomposites added 25 wt% ZnS nanoparticles (a) Before acid immersion, (b) After acid immersion.

the pseudo-first-order model for the linear plots of prepared ceramics nanocomposite were very close to 1. Results indicated that the photocatalytic degradation kinetics could be effectively explained by this pseudo-first-order model. All experimental data had similar  $R^2$  values (0.986–0.996), indicating that the typical behavior of a pseudo-first order model perfectly follows a straight line. In addition,  $k_1$  values of the acid treated ceramics nanocomposite added with 25.0 wt% ZnS for MO, ATA, 2,4-D, and MB were  $0.139\ \text{min}^{-1}$ ,  $0.162\ \text{min}^{-1}$ ,  $0.148\ \text{min}^{-1}$ , and  $0.134\ \text{min}^{-1}$ , respectively. These results demonstrate that the ceramic nanocomposites produced can be applied to a number of different environments and chemical engineering fields substantially.

Fig. 7 represents the photoluminescence (PL) spectra of ceramic nanocomposites (before and after acid treatment) with increasing ZnS nanoparticle content.

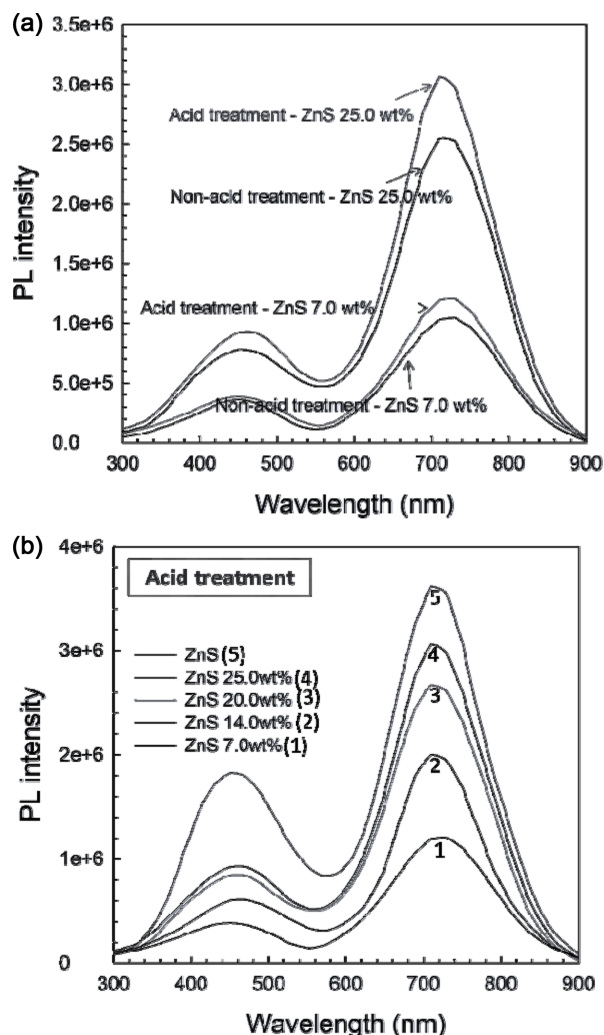


**Fig. 7.** Photoluminescence (PL) spectra of the prepared ceramic nanocomposites. (a) PL spectra of the ceramic nanocomposites added 7 and 25 wt% ZnS with/without acid immersion. (b) PL spectra of the ceramic nanocomposites added ZnS nanoparticles; 0, 7, 14, 20, and 25 wt% (after acid immersion).

As shown in Fig. 7a, when compared with the PL spectra intensity of acid and non-acid treated ceramic nanocomposites added 7.0 and 25.0 wt% ZnS nanoparticles, the PL spectra intensity was higher for nanocomposites after acid treatment. Results showed a significant increase in photoactivity after acid treatment. In addition, the PL spectra of acid-treated ceramic nanocomposites manufactured with increasing content of ZnS increased in intensity at 720.0 nm as the specific peak of ZnS (Fig. 7b). The reason is judged that the intensity of the specific peak was increased because the pores and specific surface of the prepared ceramic ZnS nanocomposite are increased by the acid treatment. From the results, it can be found that the photocatalytic activity for photodegradation targets was increased. From these results, it could be verified that the photocatalytic activity of ceramic nanocomposites is determined to be nanomaterials with the utility and

benefits of these ZnS nanoparticles.

## Conclusions

In this study, ceramic ZnS nanocomposites were manufactured using fly ash, waste glass powder, and ZnS nanoparticles. According to FE-SEM analysis, for ceramic ZnS nanocomposites with ZnS content of 20.0 and 25.0 wt%, the alteration of irregular-type ZnS nanoparticles in the nanocomposite matrix was not different between before and after acid treatment. It showed an adequate improvement in chemical durability with good enough mechanical properties under all conditions. When the ZnS content was increased from 0 to 25.0 wt%, the compressive and bending strength were increased by 150.8 MPa and 65.8 MPa (after immersing in acidic solution), respectively. The analysis results indicated that the addition of ZnS nanoparticles could advance the mechanical properties of ceramic nanocomposites. The physical properties of ceramic nanocomposites were improved because the addition of ZnS nanoparticles resulted in specific matrix-strengthening arrangements formed between components. The photocatalytic degradation of ZnS-added ceramic nanocomposites was investigated using MO, ATA, 2,4-D, and MB as photodegradation targets under UV irradiation. All ceramic nanocomposites in which ZnS nanoparticles were added showed photocatalytic activity under UV light irradiation.

## Acknowledgments

This work was supported by the Basic Science Research Program through the National Research Foundation of Korea (NRF) funded by the Ministry of Education (2019R111A3A01061508).

## References

- G.J. Lee and J.J. Wu, *Powder Technol.* 318 (2017) 8-22.
- J.S. Hu, L.L. Ren, Y.G. Guo, H.P. Liang, A.M. Cao, L.J. Wan, and C.L. Bai, *Angew. Chem. Int. Ed.* 44 (2005) 1269-1273.
- P. D'Amico, A. Calzolari, A. Ruini, and A. Catellani, *Sci. Rep.* 7 (2017) 16805-16812.
- V. Dimitrova and J. Tate, *Thin Solid Films* 365 (2000) 134-138.
- H. Chander, V. Shanker, D. Haranath, S. Dudeja, and P. Sharma, *Mater. Res. Bull.* 38 (2003) 279-288.
- M. Bredol and M. Kaczmarek, *J. Phys. Chem. A* 114 (2010) 3950-3955.
- M. Bredol, M. Kaczmarek, and H.D. Wiemhöfer, *J. Power Sources* 255 (2014) 260-265.
- J.P. Borah and K.C. Sarma, *Acta. Phys. Pol. A* 114 (2008) 713-719.
- X. Xu, S. Li, J. Chen, S. Cai, Z. Long, and X. Fang, *Adv. Funct. Mater.* 28 (2018) 1802029.
- I. Altın, I. Polat, E. Bacaksız, and M. Sokmen, *Appl. Surf. Sci.* 258 (2012) 4861-4865.

11. L. Kashinath, K. Namratha, and K. Byrappa, *J. Alloys Compd.* 695 (2016) 799-809.
12. E.G. Barojas, E.S. Mora, C.C. Abriz, E.F. Rodríguez, and R.S. González, *J. Supercond. Nov. Magn.* 26 (2013) 2337-2340.
13. K.K. Senapati, C. Borgohain, and P. Phukan, *Catal. Sci. Technol.* 2 (2012) 2361-2366.
14. Z. Zhang, C. Fang, X. Bing, and Y. Lei, *Materials* 11 (2018) 512-519.
15. E.H. Song, B.H. Kang, T.Y. Kim, H.J. Lee, Y.W. Park, Y.C. Kim, and B.K. Ju, *ACS Appl. Mater. Interfaces* 7 (2015) 4778-4783.
16. C.Y. Lai, A. Groth, S. Gray, and M. Duke, *Water Res.* 57 (2014) 56-66.
17. S.D. Yoon and Y.H. Yun, *J. Ceram. Process. Res.* 12 (2011) 361-364
18. J.Y. Park, D.Y. Choi, K.J. Hwang, S.J. Park, S.D. Yoon, Y.H. Yun, X.G. Zhao, H.B. Gu, and I.H. Lee, *J. Nanosci. Nanotechnol.* 15 (2015) 5224-5227.
19. Y.H. Yun, K.J. Hwang, Y.J. Wee, S.D. Yoon, *J. Appl. Polym. Sci.* 120 (2011) 1850-1858.
20. Y.H. Yun, C.H. Yoon, J.S. Oh, S.B. Kim, B.A. Kang, K.S. Hwang, *J. Mater. Sci.* 37 (2002) 3211-3215.
21. M.R. Hoffmann, S.T. Martin, W. Choi, D.W. Bahnemann, *Chem. Rev.* 95 (1995) 69-85.
22. H.R. Pouretedal, H. Beigy, M.H. Keshavarz, *Environ. Technol.* 31 (2010) 1183-1190
23. S. Lagergren, *Handlingar* 24 (1989) 1-39.